UDC 533.98:539.216:620.172.24

K.H. AHARONYAN, E.E. ELBAKYAN, A.Zh. KHACHATRYAN, E.P.KOKANYAN

IMPURITY-LIMITED ELECTRON SCATTERING IN $TiO_2/InSb/TiO_2$ QUANTUM WELL NANOSTRUCTURES

The effect of electronic and high-κ dielectric barrier quantum screening on the impurity-limited electron scattering in the ***$TiO_2/InSb/TiO_2$*** two-dimensional (*2D*) nanostructure is considered. An analytical calculation model corresponding to the quantum well/high-κ dielectric barrier heterostructure under discussion is presented. A numerical analysis of the screened impurity interaction potential specific to ***$InSb/TiO_2$*** heterojunction is implemented. A calculation of an electron momentum relaxation time (τ) is carried out taking info account both the finite mismatch of the energy bands at the ***$InSb/TiO_2$*** heteroboundary and the energy band non-parabolicity of the ***InSb*** material. The contributions of screened potential compound *2D* forms to τ are established and compared related to the corresponding results for the ***$HfO/InSb/HfO_2$*** *2D* nanostructure.

Keywords: quantum well, high-κ dielectric, screening, impurity scattering.

1. Introduction

At present, the inclusive investigations are supported related to physical properties of mobile two-dimensional electron gas (*2DEG*) in the narrow band gap *III–V* group semiconductor quantum wells (*QW*) joint with the high-κ dielectrics as the substrat barrier media [1]. In these *2D* structures, a high carrier mobility of nanosamples ($\sim 10^4 \div 10^5$ cm^2 V^{-1} s^{-1}) would be achieved providing the high-speed power switching, low dissipation and additional benefits of electronic nanodevices. As a result, the high-κ materials progressively replace the traditional dielectric silicon oxide in many silicon-based nanodevices. Because the material background of the *2DEG* is not certainly dielectrically homogeneous, its operation is influenced by the surrounding dielectric environment. This affects the nature of the Coulomb interaction in the active nanolayer by means of both the *2D* electronic-nature screening (*ES*) and dielectric barrier-nature screening (*DBS*) mechanisms. Accordingly, with the appropriate material and structural design of the *QW* and surrounding dielectric medium, a significant advance in the optical and transport characteristics in these nanosystems would be revealed [2, 3]. In this regard, the screened impurity scattering effect comprehensive analysis for the realistic ***$InSb/HfO_2$*** heterointerface was performed in Refs. 3 and 4 and a substantial suppression of the electron scattering was obtained. In the paper, a problem of the screened impurity scattering effect is considered inclusively in the presence of the more enhanced *DBS* mechanism on the base of ***$InSb/TiO_2$*** *QW/hh-κ* - type finite

confining potential heterointerface. The obtained results are compared with the previously obtained data in the case of ***InSb/HfO₂*** *QW/hh-κ* type finite confining potential heterostructure with a lower value of the barrier dielectric constant.

2. The model

Let us have a semiconductor *QW* with the dielectric constant ε_w and width d, neighbored by the dielectric barrier medium with a symmetrical outline of dielectric constants on both sides as $\varepsilon_b = \varepsilon_{b_2} = \varepsilon_{b_1}$. Also, a strong *QC* and high-κ *DBS* effects characterized by conditions $\square_0 >> d$ and $\varepsilon_r = \varepsilon_w / \varepsilon_b << 1$, respectively, are accepted, where the Bohr radius is $\square_0 = \varepsilon_w \square^2 / m_e e^2$, m_e –the electron effective mass. Here, only the *n*-type 2D charged channel with the average surface density n_S contributes to the impurity center screening. Certainly, we also assume that the *QW* width d is small compared with the Debye radius for bulk samples as $r_D >> d$.

As obtained in Ref.2, for the case of *QW/hh*-κ - based structure at the moderately large effective 2D distances

$$d \ll \rho \leq \varrho(\rho_s, \varepsilon_r) , \tag{2.1}$$

where $\varrho(\rho_s, \varepsilon_r) = \frac{\rho_s}{\varepsilon_r}\left[\left(\frac{e^3+1}{e^3-1}\right)^2 - \varepsilon_r^2\right]^{1/2}$, e = 2.71, a screened impurity interaction potential takes the *2D* Debye-Hückel potential form:

$$V_s(\rho) = -\frac{e^2}{\varepsilon_w}\frac{\exp(-\rho/\rho_s)}{\rho} , \tag{2.2}$$

while at the large enough 2D distances satisfying the conditions,

$$\begin{cases} \rho \gg \varrho(\rho_s, \varepsilon_r) \\ \rho > \frac{d}{2\varepsilon_r} \end{cases} , \tag{2.3}$$

is characterized by the pure *2D* potential form:

$$V_s(\rho) = -\frac{e^2}{\varepsilon_b}\left\{\frac{1}{\rho} + \pi\varepsilon_r q_s[H_0(2\varepsilon_r q_s\rho) - N_0(2\varepsilon_r q_s\rho)]\right\}, \tag{2.4}$$

In Exps. (1) - (3) ρ_s and q_s are the *2D* screening radius and *2D* screening parameter, respectively, which, according to the Thomas – Fermi method model are given as:

$$\rho_s = \sqrt{\frac{d}{2q_s}} . \tag{2.5}$$

In particular, for the degenerate and non-degenerate *2DEG* statistics the screening parameter q_s takes, correspondingly, the forms:

$$q_s = \frac{2}{a_0}\,,\; x = \frac{\pi n_S \hbar^2}{m_{ew} k_B T} >> 1 \tag{2.6}$$

and

$$q_s = \frac{2}{a_0}\frac{\pi n_S \hbar^2}{m_w k_B T}\,,\; x = \frac{\pi n_S \hbar^2}{m_w k_B T} << 1. \tag{2.7}$$

An electron momentum relaxation time due to the scattering of carriers by impurities in the relaxation time approximation is given by [3]:

$$\frac{1}{\tau} = N_s v_k \int_0^{2\pi} \sigma(\varphi)\,(1 - cos\varphi) d\varphi\,. \tag{2.8}$$

In Exp. (2.8) $N_s = N_V d$, where N_V is the *3D* density of background impurities, $v_k = \hbar k / m_w$ is the electron velocity, φ - the electron scattering angle expressed by the initial $\vec{k}$ and final $\vec{k}'$ *2D* wave vectors of a scattered electron in the *QW* plane as $cos\varphi = \frac{\vec{k}\vec{k}'}{|\vec{k}||\vec{k}'|}$. Here $\sigma(\varphi)$, determining a *2D* flux of particles scattered at the angle φ, for the *2D* screened impurity potential forms after Exps.(2.2) and (2.4) correspondingly takes the calculated expressions [3, 4]:

$$\sigma(\varphi) = \frac{2\pi m_w e^4}{\varepsilon_w^2 \hbar^3 v_k} \frac{\rho_s^2}{1 + 2\,k^2 \rho_s^2 (1 - cos\varphi)} \tag{2.9}$$

and

$$(\varphi) = \rho_0 \left| \frac{1}{\sqrt{\pi}} exp\left(\frac{\pi}{2\varepsilon_r a_o k}\right) \Gamma\left(\frac{1}{2} - \frac{i}{\varepsilon_r a_o k}\right)\; {}_1F_1\left(\frac{i}{\varepsilon_r a_o k}, \frac{1}{2}, ik\rho_0(1 - cos\varphi)\right) - 1 \right|^2. \tag{2.10}$$

To obtain Exp.(2.10), a cut-off Coulomb potential is used:

$$V_s^K(\rho) = \begin{cases} \frac{c_1 e^2}{\varepsilon_b \rho} & \rho \le \rho_0 \\ 0 & \rho > \rho_0 \end{cases}, \tag{2.11}$$

where $\rho_0 = c_2 \varrho(\rho_s, \varepsilon_r)$ and c_1, c_2 are the simulation parameters ensuring the continuity of impurity interaction potential $V_s(\rho)$.

Because we are dealing with the narrow band gap *III–V* group semiconductor *QW*, it is consequently required to take into account the nonparabolicity *(NP)* effect on m^*_e in order to evaluate τ more precisely. Within the Kane model, the conduction energy band can be described by the dispersion equation:

$$E\left(1 + \frac{E}{E_g}\right) = \frac{\hbar^2 k_w^2}{2 m^*_{ew}}\,, \tag{2.12}$$

where E is the electron energy. In Exp. (2.12) the electron wave vector k_w has the direction normal to *QW* plain and might be defined from the secular equation:

$$tg\left(\frac{k_w d}{2}\right) = \frac{m_w(E)}{m_b^*}\frac{k_b}{k_w} \tag{2.13}$$

related to the rectangular band *QW/dielectric barrier* system. Here, the wave vectors k_w and k_b in the *QW* and barrier regions with the conduction band offset Δ^c are defined as:

$$k_w^2 = 2\frac{m_w(E)\,E}{\hbar^2} \text{ and } k_b^2 = 2\frac{m_b(\Delta^c - E)}{\hbar^2}, \tag{2.14}$$

where m_b is the electron effective mass in the barrier region. In Exp. (2.13) the energy-dependent effective mass $m_w(E)$ is related to the first derivative of the dispersion relation with respect to wave vector as:

$$m_w(E) = \hbar^2 k_w^2 \frac{\partial k_w}{\partial E}. \tag{2.15}$$

From Exps.(2.12) - (2.15), bearing in mind that Δ^c is large related to *Egw,* we come to the *NP* corrected electron effective mass expression $m_w(E) = m_e^* m_{NP}$ with the characteristic *NP* parameter m_{NP} as:

$$m_{NP} = \sqrt{1 + 2\frac{\hbar^2 k_w^2}{m_e^* E_g^w}}. \tag{2.16}$$

3. The impurity-limited electron scattering time under the *InSb/TiO₂ QW/hh-κ -type* heterointerface

Let us now, based on the presented physical model, proceed to a numerical analysis of the impurity-limited electron scattering time related to the ***TiO₂/InSb/TiO₂*** prospective *QW*/high-κ dielectric barrier structure, wherein, for the ***InSb/TiO₂*** interface, the dielectric constant ratio $\varepsilon_r = \varepsilon_w/\varepsilon_b = \varepsilon_{InSb}/\varepsilon_{TiO_2}\big|_{a\ axes} \approx 16.8/90 \approx 0.19$ is taken [5]. In accordance with the strong QC condition $\square_0 >> d$, we will display a numerical data for the *QW* width values $d < 10$ nm, bearing in mind, that *InSb* bulk sample holds a macroscopically large impurity effective Bohr radius as $\square_0 \approx 64$ nm due to the smallest electron effective mass ($m^*_e \approx 0.014\ m_0$, m_0 the free electron mass)). In particular, the calculations are carried out for the *QW* width fixed value as $d = 2$ *nm* correlated with the *2DEG* characteristic parameter value as $n_s/T\,|_1 = 3.3.10^8\ cm^{-2}/{}^0K$ (electron *2D* density $n_s \approx 1.10^{11}\ cm^{-2}$ at $T \approx 300\ {}^0K$) corresponding to nondegenerate type of *2DEG* (with the nondegeneracy parameter $\pi n_s \hbar^2/m_w k_B T|_1 \approx 0.11$). In calculations, we admit that the background impurity scatterers are distributed with the same in-plain density as *2DEG* electrons ($N_s = n_s$). As known, the conduction band of ***InSb*** material is highly non-parabolic due to a narrow band gap ($\approx 0.17eV$ under $T=300^0K$), and so the electron effective mass m^*_{ew} becomes energy-dependent with the appropriate conduction (*c*) and valence

(*v*) band offsets which, for the ***TiO₂/InSb/TiO₂*** *QW*/high-κ dielectric barrier structure, are demonstrated in Table. For comparison, analogous data for the ***HfO₂/InSb/HfO₂*** *QW*/high-κ dielectric barrier structure are shown as well.

Table

The used and calculated numerical results of the TiO_2/InSb/TiO_2 and HfO_2/InSb/HfO_2 QW/high - κ - type nanostructures

	TiO₂	***HfO₂***
m_b *)	*0.7 m_0* [6, 7]	*0.6 m_0 [8]*
$\varepsilon_r = \varepsilon_w / \varepsilon_b$	16.8 /90$|_{\text{a axes}}$ ≈ 0.19 [5]	*16.9 / 27 ≈ 0.62*
E_{gb}	*3.1 eV (300K⁰)* [6, 7]	*5.3 eV (300K⁰)* [8]
Δ_c **)	*1 eV*	*1.78 eV(300K⁰) [9]*
$k_w d$	*1.128*	*1.5*
m^{fin}_{eNP}	*4.65*	*6.11*
$c_1\|_{m_w(E)}$	*0.006*	*0.245*
$c_2\|_{m_w(E)}$	*960*	*5.25*

*) The barrier electron effective mass is taken for the ***TiO₂*** (***rutile)*** polymorph material related to the Γ→ Z direction in the Brillouin zone [6, 7].

) Due to the absence of clear data on the conduction band offset Δ_c for such a *QW* system, we deal here with a compromised value of $\Delta_c \approx$ *1 eV* which is received by extrapolation of the analogous value for the ***HfO₂/InSb/HfO₂* *QW/hh*-κ type nanostructure (see Table) [3].

In Fig. 1, the screened interaction potential $V_s(\rho)$ graphs according to Exps (2.2) and (2.11) are shown. Here, the solid and dashed lines refer to the ***TiO₂/InSb/TiO₂*** and ***HfO₂/InSb/HfO₂*** *QW/high* – κ- type nanostructures, respectively. Aset follows, an increase in the dielectric constant of the surrounding *QW* medium, according to the outline $\varepsilon_b|_{HfO_2} \approx 27 \rightarrow \varepsilon_b|_{TiO_2} \approx 90|_{\text{a axes}}$, leads to a significant rearrangement of the $V_s(\rho)$ screened interaction potential graphic picture. As we can see, a graphical pattern in the ***TiO₂/InSb/TiO₂*** *QW/hh-κ-* type finite confining potential heterostructure case, with the higher barrier dielectric constant, $\varepsilon_b \approx 90|_{\text{a axes}}$, is predominantly formed by the screened impurity potential $V_s(\rho)$ particular type V_s^{DH} (Exp.(2.2)), and starting from the *2D* distance value $\rho/a_0 \approx$ *0.77* (marked by the dashed-dotted vertical line in Fig.1) and more, a screened potential particular type V_s^K (Exp.(2.11)) only becomes effectively adopted. Besides that, in the *2D* distance interval $\rho/a_0 <$ *0.77* an intensity of screened interaction drops already to the negligible values. On the whole, this indicates that for the entire *2D* distance allowed interval $\rho \gg d$, the main contribution to the screened interaction

is formed by V_s^{DH} particular type of screened impurity potential $V_s(\rho)$. This indicates that, with the moderate large distances $\rho/a_0 < 0.77$, the Coulomb field lines become increasingly concentrated in the *QW* region. As follows, here, the *QW* material dielectric constant is decisive and, thus, V_s^{DH} potential type becomes effective.

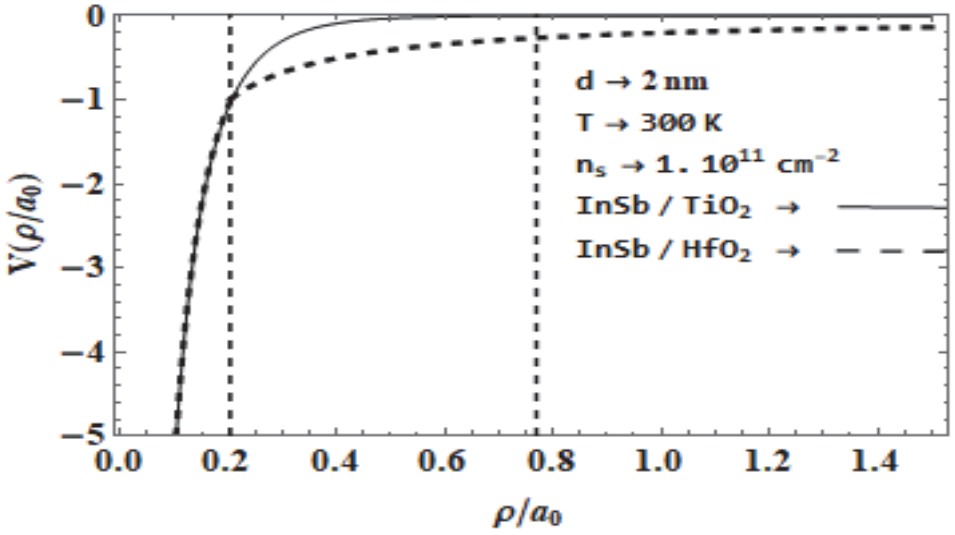

Fig. 1. The screened interaction potential $V_s(\rho/a_0)$ dependence for $TiO_2/InSb/TiO_2$ and $HfO_2/InSb/HfO_2$ QW/hh-κ type nanostructures in the case of d = 2 nm with non-degenerate 2DEG ($n_s/T \approx 3.3.10^8$ $cm^{-2}/^0K$) at a background impurity density $N_S \approx 1.10^{11}$ cm^{-2}

In turn, for the case of ***HfO_2 / InSb / HfO_2*** *QW/hh-κ* - type structure with the lower than in the former case dielectric constant ($\varepsilon_b \approx 27$), a characteristic transition edge (marked by the dashed-dotted vertical line with $\rho/a_0 \approx 0.2$ data in Fig.1) between the $V_s(\rho)$ screened potential particular types V_s^{DH} and V_s^K is shifted to the lower values of ρ/a_0 parameter in accordance with the validity criteria after Exps. (2.1) and (2.3). The latter effectively leads to an increase in both the *2D* distance allowed interval of V_s^K potential form and their noticeable contribution in the $V_s(\rho)$ reaches until the values of 1 *meV*. This indicates that despite the decrease of ε_b for the ***HfO_2/InSb/HfO_2*** *QW/hh-κ* type structure, with the moderate large distances $\rho/a_0 < 0.2$, the Coulomb field lines are increasingly concentrated in the *QW* region. As it follows, here, as in the former case, the *QW* material dielectric constant is decisive and the V_s^{DH} potential type is effective again.

In calculations, a continuity of the graphic curves is provided by the simulation of the parameters c_1 and c_2 (see both the Exp.(2.11) and Table). Such displacement indicates that, for the thin enough *QW* samples ($d = 2nm$), in the

corresponding *2D* distance ρ, the surrounding medium dielectric constant ε_b becomes a key factor. The latter illustrates a physical situation that with the small values of *QW* width *d*, at the corresponding distances ρ from the impurity, a dominant part of the screening Coulomb field extending beyond the confinement region passes through a barrier media characterized by the *high* -κ value dielectric constant ε_b. Note that, a determination of the specified transition edge position between the allowed intervals of the used potential forms can be of both *practical* importance for characterizing the role of the *ES* and *DS* mechanisms in the efficiency of the scattering process and of *fundamental* significance to revealing the design pattern of the screened Coulomb interaction in the *QW* system under discussion.

Let us now, on the basis of the demonstrated data of the screened Coulomb interaction in the discussed *QW/hh-κ* - type finite confining potential nanostructures consider the momentum relaxation time $\tau(ka_0)$ dependence on the basis of Exp. (2.8).

The graphs obtained in Fig.2 are a result of contributions from both screened impurity potential types after Exp.(2.2) and Exp.(2.11) related to different intervals of ka_0 parameter. The latter are located in the right and left sides of the transition edges (marked by dashed vertical lines on Fig.2), respectively. Such an integrated picture proceeds from the relationship between the material parameters of the ***InSb/TiO₂*** and ***InSb/HfO₂*** *QW/high-κ* heterojunctions, which, as already noted above, touches upon the acting region duration of a particular type of the screened impurity potential. In particular, as shown in Fig.2, a transition edge between the two aforementioned forms of potential for the graph with ***InSb/TiO₂*** case corresponds to the $ka_0 \approx 1.3$ value, while for the ***InSb/HfO₂*** case it corresponds to the $ka_0 \approx 4.92$ value. Thus, a shift of the transition edge takes place towards the smaller wave vector values with the increase of the surrounding medium dielectric constant ε_b ($\varepsilon_b|_{HfO_2} \approx 27 \rightarrow \varepsilon_b|_{TiO_2} \approx 90|_{\text{a axes}}$) in accordance with the validity criteria after Exps. (2.1) and (2.3).This shift indicates that as ε_b decreases, for larger and larger *2D* electron wave vector values (with a corresponding decrease in *2D* distances ρ), the surrounding medium dielectric constant ε_b becomes a key factor. In turn, as a consequence of the latter, with the reasonable effective values of $ka_0 > 0.1$ a τ graphic line for the ***InSb/HfO₂*** case is characterized by oscillation behavior while in the ***InSb/TiO₂*** case a monotonic decrease of τ is observed.

In Fig.2 a graphic line corresponding to the *ES* effect - absent case in the dielectrically homogenous ***InSb/AlInSb*** *QW* structure is shown. As it follows, a strong suppression of electron impurity scattering process is revealed when taking into account the *ES* and *DBS* effects simultaneously in the discussed structures with the *QW/high-κ* heterojunctions. Wherein this suppression effect, expressed by an

increase in τ, is quite essential (by an order of magnitude) for the region $ka_0 < 3$ corresponding to the relaxation time interval $\tau < 5.5.10^{-14}$ s.

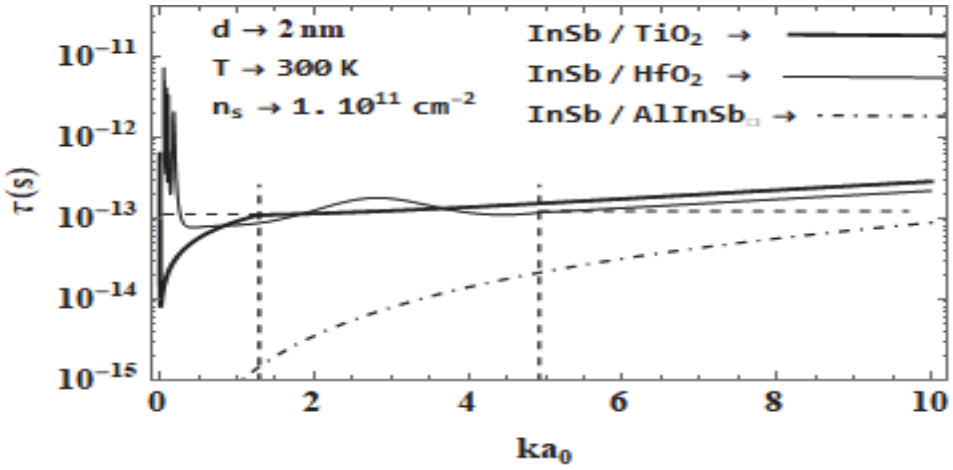

*Fig. 2. Electron momentum relaxation time $\tau(ka_0)$ dependence for the **TiO_2/InSb/TiO_2** and **HfO_2/InSb/HfO_2** QW/hh-κ type nanostructures in the cases of d = 2 nm with non-degenerate 2DEG ($n_s/T \approx 3.3.10^8$ $cm^{-2}/^0K$) at a background impurities density of $N_S \approx 1.10^{11}$ cm^{-2}. The graph corresponding to the BS and ES effect absent case in the **InSb/AlInSb** QW nanostructure is at the bottom (dashed-dotted line)*

REFERENCES

1. **Robertson J., Wallace R.** High-K materials and Metal Gates for CMOS applications // Mater. Sci. and Eng.: R: Rep.- 2015.-V. 88.-P.1-41.
2. **Aharonyan K.H., Kazaryan E.M., Kokanyan E.P.** Screened shallow impurity properties of quantum well heterosystems with high-κ dielectric barrier environment // Physica E.-2019.-V.113.-P. 47-53.
3. **Aharonyan K.H., Kazaryan E.M., Bazzan M., Kokanyan E.P.** Screened shallow impurity properties of quantum well heterosystems with high-κ dielectric barrier environment // Physica B.-2024.-V.695.-P. 416535-1-8.
4. **Aharonyan K.H., Khachatryan A.Zh., Kokanyan E.P.** Screened impurity scattering relaxation time with the quantum well/high-κ dielectric heterojunction // National Polytechnic University of Armenia Bulletin .-2023.-V.1.-P.48-54.
5. On the permittivity of titanium dioxide /**J. Bonkerud, Ch. Zimmermann, Ph. M. Weiser, et al** // Sci. Rep.-2021.-V.11.- P. 12443-1-5.
6. **Ekuma Ch.E., Bagayoko D.** Ab-initio Electronic and Structural Properties of Rutile Titanium Dioxide // Jpn.J.Appl.Phys.- 2011.-V.50.- P. 101103 1-25.
7. **Perevalov T.P., Gritsenko V.A.** Electronic Structure of TiO2 Rutile with Oxygen Vacancies: Ab Initio Simulations and Comparison with the Experiment // JETP.- 2011.- V. 112.-P.310-316.

8. Demonstrating 1 nm-oxide-equivalent-thickness HfO_2/InSb structure with unpinning Fermi level and low gate leakage current density /**H.-D. Trinh, et al** // Appl.Phys.Lett.- 2013.-V.103.- P.142903-1-5.
9. **Gritsenko V.A., Perevalov T.V., Islamov D.R.** Electronic properties of hafnium oxide: A contribution from defects and traps // Physics Reports.- 2016.-V. 613.-P. 1-20.

Կ.Հ. ԱՀԱՐՈՆՅԱՆ, Է.Ե. ԷԼԲԱԿՅԱՆ, Ա.Ժ. ԽԱՉԱՏՐՅԱՆ, Է.Պ. ԿՈԿԱՆՅԱՆ

ԽԱՌՆՈՒԿԱՅԻՆ ՍԱՀՄԱՆԱՓԱԿՄԱՄԲ ԷԼԵԿՏՐՈՆՆԵՐԻ ՑՐՈՒՄԸ $TiO_2/InSb/TiO_2$ ՔՎԱՆՏԱՅԻՆ ՀՈՐՈՎ ՆԱՆՈԿԱՌՈՒՑՎԱԾՔՆԵՐՈՒՄ

Քննարկվել է էլեկտրոնային և բարձր-κ դիէլեկտրական արգելքային բնույթների քվանտային էկրանավորման ազդեցությունը էլեկտրոնների խառնուկային սահմանափակմամբ ցրման վրա $TiO_2/InSb/TiO_2$ երկչափ (*2D*) նանոկառուցվածքում: Ներկայացվել է դիտարկված քվանտային հոր/բարձր -κ դիէլեկտրական արգելք հետերոկառուցվածքին համապատասխանող վերլուծական հաշվարկային մոդել: Իրականացվել է $InSb/TiO_2$ հետերոանցմանը բնորոշ էկրանավորված խառնուկային փոխազդեցության պոտենցիալի թվային վերլուծություն: Կատարվել է ցրման վերակագնման ժամանակի (τ) թվային հաշվարկ՝ հաշվի առնելով ինչպես $InSb/TiO_2$ հետերոսահմանում էներգիական գոտիների վերջավոր կապակցումը, այնպես էլ *InSb* նյութի էներգիական գոտիների ոչ պարաբոլականությունը: Հաստատվել են էկրանավորման պոտենցիալի *2D* բաղադրիչ տեսքերի ներդրումները τ-ի մեջ, և համեմատվել են $HfO/InSb/HfO_2$ *2D* նանոկառուցվածքին բնորոշ համապատասխան արդյունքների հետ:

Առանցքային բառեր. քվանտային հոր, բարձր-κ դիէլեկտրիկ, էկրանավորում, խառնուկային ցրում:

К.Г. АГАРОНЯН, Э.Е. ЭЛБАКЯН, А.Ж. ХАЧАТРЯН, Э.П. КОКАНЯН

ПРИМЕСНО-ОГРАНИЧЕННОЕ РАССЕЯНИЕ ЭЛЕКТРОНОВ В НАНОСТРУКТУРАХ С КВАНТОВЫМИ ЯМАМИ $TiO_2/InSb/TiO_2$

Рассмотрено влияние электронного и высокого-κ диэлектрически барьерного типов квантового экранирования на примесно-ограниченное рассеяние электронов в двумерной (2D) наноструктуре $TiO_2/InSb/TiO_2$**.** Представлена аналитическая расчетная модель, соответствующая обсуждаемой гетероструктуре типа “квантовая яма/высокий-κ диэлектрический барьер”. Реализован численный анализ экранированного примесного потенциала взаимодействия, специфичного для гетероперехода $InSb/TiO_2$. Проведен численный расчет времени релаксации импульса электрона (τ) с учетом как конечного разрыва энергетических зон на гетерогранице $InSb/TiO_2$, так и непараболичности энергетических зон материала ***InSb***. Установлены вклады *2D* составных форм экранированного потенциала в τ, проведено их сравнение с соответствующими результатами для *2D* наноструктуры $HfO/InSb/HfO_2$.

Ключевые слова: квантовая яма, высокий-κ диэлектрик, экранирование, примесное рассеяние.